J. Fluid Mech. (1982), *vol.* 114, *pp.* 187–211
Printed in Great Britain

Collapsible tube model for the dynamics of closure of the mitral valve

By M. BITBOL, Ph. DANTAN, P. PERROT AND C. ODDOU

Laboratoire de Biorhéologie et d'Hydrodynamique Physiologique, E.R.A. CNRS 662, Université Paris VII – T. 33/34, 2, Place Jussieu 75251 Paris Cedex 05

(Received 30 May 1980 and in revised form 31 December 1980)

The fluid mechanics of the closure motion of a short collapsible tube segment, subject to a strong flow deceleration as in one of Henderson & Johnson's (1912) experiments, is investigated experimentally and theoretically. Physical similarity to the closure process of the mitral valve is obtained. In the study particular emphasis is placed upon the evolution of the longitudinal profiles of the collapsible tube during its closure motion. It is found that the flexible tube first closes near its upstream end and that this first phase is followed by a propagation process toward the downstream end. The characteristics of this typical sequence and of the longitudinal shape of the collapsible tube are related to hydrodynamic parameters. The results predicted by the theory agree consistently with those obtained from the experiments.

1. Introduction

In the past, many explanations of the mitral-valve closure mechanism have been presented. Most of the recent interpretations have been based on the hypothesis that the valves are essentially dependent upon fluid-dynamic processes.

It was Leonardo da Vinci (1513) who first suggested a hydrodynamical mechanism for the closure of the heart valves. Leonardo's interpretation indicated that the valves could be closed by means of the vortical flow field, which is present in the ventricle during diastole and in the aortic sinus during systole. This concept was re-examined and analysed both mathematically and experimentally by Bellhouse & Talbot (1969) and Bellhouse (1972) and nowadays this type of explanation of heart valve closure is much debated.

Yellin *et al.* (1976) made the remark that the order of magnitude of the maximal filling velocity does not allow the intraventricular fluid to achieve a complete re-circulation process inside the ventricular cavity, at least not during the first phase of diastole (rapid filling phase). This concept contrasts with the assumption that the recirculation ring plays the main role in mitral-valve closure.

The mitral valve is indeed partially closed after deceleration of the fluid, which takes place at the end of the first phase of diastolic filling, in spite of the supposed absence of any vortical field.

However, the arguments concerning the sequence of vortex ring generation during diastole are not entirely conclusive. This was shown in both numerical (Oddou *et al.* 1979) and *in vivo* experimental studies (Brun *et al.* 1980), which demonstrated that slight vortical recirculation appears very early during the first diastolic phase, and

then grows and persists throughout diastole. Their presence could thus allow them to play an important role in the dynamics of the valves. Can this be considered an adequate reason for accepting the vortex interpretation of heart valve closure?

Two recent experimental hydromechanical models have yielded opposite conclusions concerning this. The experiments reported by Bellhouse (1972) showed that the increase in ventricle volume, which induces a decrease in vortex strength, also implies delayed mitral-valve closure and an increased amount of regurgitated flow. It was concluded that the eddies which develop in the left ventricle before mitral-valve closure play an essential role in subsequent mitral-valve closure. Recent experiments carried out by Reul & Talukder (1979) showed, however, that the decrease in vortex strength around the valve does not influence its closure motion.

This divergence is readily explained if we notice with Lee & Talbot (1979) that in Bellhouse's experiments flow deceleration through the valve was consistently lower than in physiological cases. In Reul & Talukder's experiments, in contrast, the hydrodynamic data agreed closely with the physiological data.

As was noticed by Bitbol *et al.* (1979) and Bitbol (1980), this divergence may also be expressed by the evaluation of a Strouhal number associated with the deceleration phase: $S = L/U_{\max}T_D$, L being the length of the valve leaflet, $U_{\max}$ the maximal velocity reached by the fluid through the mitral ring, and T_D the time required by the fluid to decelerate from $U_{\max}$ to zero. In Bellhouse's experiments, S was equal to 0·1 whereas in the experiments of Lee & Talbot and Reul & Talukder $S \simeq 1$, which is a characteristic value of physiological conditions.

This essential difference between the values of the Strouhal number does not appear any longer if, like most physiologists, one uses the period of the cardiac cycle instead of the duration of deceleration, to define the Strouhal number. Its value is, in this case, always close to 0·03.

The meaning of the Strouhal-number characteristic of the deceleration phase underlines the importance of this difference. $S = L/U_{\max}T_D$ can be interpreted as the ratio between the valve length and the maximal distance covered by the fluid during the deceleration period. When $S \ll 1$, most of the hydrodynamic phenomena occurring during the deceleration phase, especially those related to the closure of the valve, take place inside the overall ventricular cavity, whereas when $S \geqslant 1$ these phenomena take place mainly in close vicinity of the valve.

The Strouhal number can also be considered as a ratio between the unsteady inertial effects and the convective inertial effects, in the equation of motion: $S = (U_{\max}/T_D)/(U^2_{\max}/L)$. When $S \geqslant 1$, as in the physiological case, the effects induced by flow deceleration through the mitral orifice are dominant.

This discussion, together with recent advances made toward a better understanding of mitral-valve dynamics, highlight the importance of the pioneering work carried out by Henderson & Johnson in 1912.

Such experiments clearly demonstrated the fact that the fast deceleration of a jet flow is sufficient to induce the closure of a piece of collapsible tube considered as a mitral-valve model. It is to be noticed that this process did not require any vortical recirculating flow, since Henderson & Johnson immersed their collapsible tube in a very large tank. These qualitative experimental results, interpreted thoroughly by Henderson & Johnson in terms of 'breaking of a jet', have been used by most of the researchers who have recently worked on this subject as an illustration of a closure

mechanism dominated by pressure gradients induced by atrio-ventricular fluid deceleration.

A complete physical analysis of the same type of hydromechanical model as the one already used by Henderson & Johnson thus appeared to be necessary. Moreover, few investigators have until now approached the subject of the evolution of the longitudinal profile of the valve leaflet during the cardiac cycle. Some of them were interested in the theoretical study of this profile during the opening phase: in this case the behaviour of the valvular leaflet may be represented as a set of Lagrangian neutrally buoyant particles linked to each other. Gillani (1974), Gillani & Swanson (1976) and Oddou *et al.* (1979) carried out numerical studies of this type, the former with an aortic-valve model, and the latter with a mitral-valve model. One should also take into account Peskin's numerical model (1977) which enabled him to explore the shape of a model of the valve leaflets, in two-dimensional geometry, throughout all the phases of the cardiac cycle. Nevertheless, the restriction of this model to values of Reynolds number which are much smaller than those encountered in the physiological case, did not enable Peskin to account satisfactorily for the important inertia-dominated effects.

Our knowledge concerning mitral-valve profiles would probably be very useful for clinical applications if new echocardiographic methods (Vogel *et al.* 1978, 1979; Brun *et al.* 1977, 1980), which have made possible real-time imaging of the entire valvular cusp, were widely used.

For all these reasons, we present in what follows a hydrodynamic analysis, both theoretical and experimental, of a simple mitral-valve model very similar to Henderson & Johnson's. Its focal point is a study of the longitudinal profile of the flexible tube which is considered to be a mitral-valve model. This longitudinal shape is correlated with hydrodynamic parameters.

2. Experiments

A mechanical model bearing physical similarity to the dynamics of mitral valve closure was used in our experimental investigations, which are reported in detail by Bitbol (1980).

The experimental device is illustrated in figure 1. It consisted of a cubic tank, filled with water, made of Plexiglas (each of its sides is 30 cm long); a rigid vertical tube made of Plexiglas of internal radius 0·8 cm with its lower end a distance l below the water level in the tank (5 cm $\leqslant l \leqslant$ 10 cm); a piece of flexible tube made of silicone rubber of length L such that 5 cm $\leqslant L \leqslant$ 10 cm. The tube's radius at rest (or when unconstrained) was $R' = 1{\cdot}03$ cm (defined as the unconstrained perimeter divided by 2π); it had a Young's modulus of approximately: $E \simeq 2 \times 10^6$ N m^{-2}, and its thickness was $h_0 = 5 \times 10^{-2}$ cm. It was fastened to the lower end of the rigid tube.

The water level was raised within the rigid tube to the height Y_0 (5 cm $\leqslant Y_0 \leqslant$ 30 cm) and maintained at that height by closing an electromagnetic gate. The gate was then opened, allowing the water column to fall. The process of the fall of the water column was divided into two phases: firstly, an acceleration phase, up to the instant when the water level in the rigid tube had reached that of the tank; secondly, a deceleration phase from the moment when the two water levels became equal. The closure of the collapsible tube takes place during the deceleration phase.

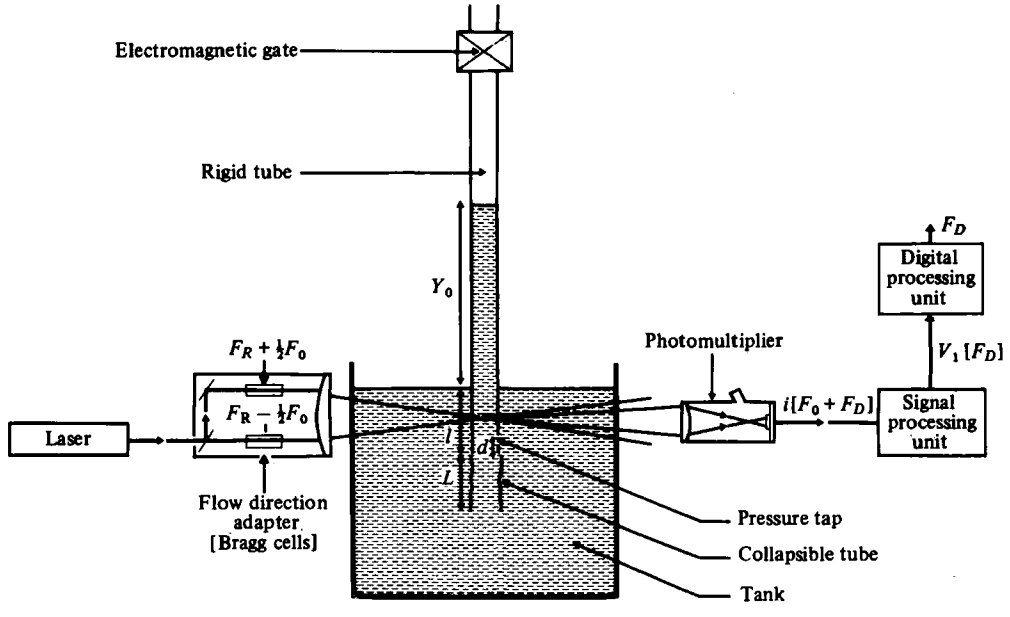

FIGURE 1. Hydromechanical model and measuring device.

Some dimensionless numbers characteristic of our experimental conditions may be evaluated. The average Reynolds number, which is defined by $Re = \bar{u}R'/\nu$, where $\bar{u}$ is the time-averaged velocity of the water column, is included within the interval [1500, 4000].

The Strouhal deceleration number $S = L/U_{\max}T_D$ is included within the interval [0·5, 2].

Finally the frequency parameter $\alpha = R'/(\nu T)^{\frac{1}{2}}$ is included within [15, 30]; T is a characteristic period of the fall ($T = (l/g)^{\frac{1}{2}}$). We must stress here the fact that these values are close to those of haemodynamic data.

The pressure within the rigid tube was measured at a distance $d = 0{\cdot}5$ cm above its lower end. A Gould–Statham P23 ID pressure transducer was used; the measurements were monitored on an Intertechnique-Plurimat S computer. Longitudinal velocity measurements were carried out on the axis of the rigid tube by means of a directional laser–Doppler velocimeter in the dual beam, forward-scatter mode (DISA). In addition, films were made using rapid cinematography (1000 images s^{-1}), allowing us to observe the closure of the collapsible tube in its collapsing plane or in a slightly oblique plane (figure 2).

The apparent instantaneous diameters of the collapsible tube were measured during closure. The image of the flexible tube was projected on to a screen made of graph paper, by means of a film analysis projector. The measurements were taken at ten equidistant points along the longitudinal co-ordinate, and each 5 ms apart.

These apparent diameters were related to the areas of the horizontal cross-sections of the collapsible tube. This relationship was found from the results of another experiment shown in figure 3: the device (1) consists of a U-tube on which a vertical collapsible tube is fastened. This collapsible tube is filled with air and plugged at its upper end. Its length is $e = 1{\cdot}05$ m. The U-tube is filled with water and a tap controls

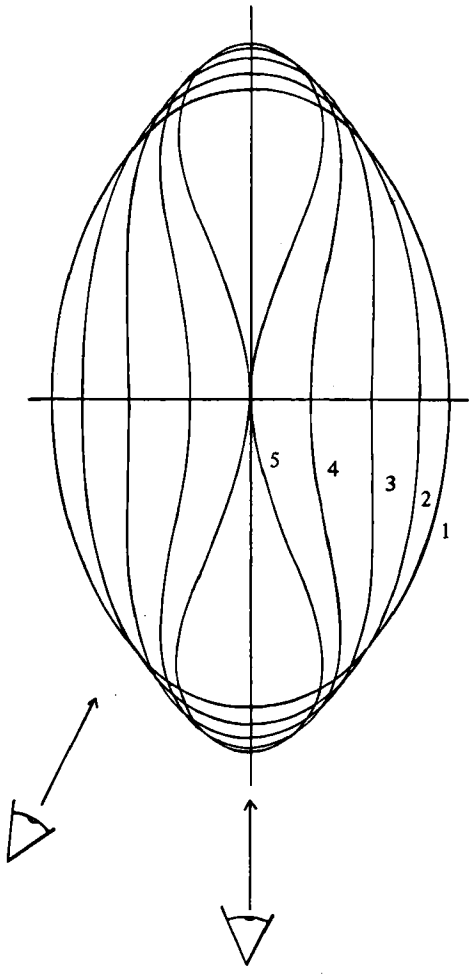

FIGURE 2. Horizontal cross-sections of the collapsible tube for different times of the closure process (from Ribreau & Bonis 1978). Two filming angles are symbolized by arrows.

the variation of the heights h and h'. For given values of h and h', the apparent diameter of the collapsible tube is measured in its collapsing plane (3). At zero transmural pressure, when $h = h'$, the area of the collapsible tube horizontal cross-section which has an elliptical shape is approximately determined by $A_0'' = \pi a(P_m^2/2\pi^2 - a^2)^{\frac{1}{2}}$, where $2a$ is the length of the small axis of the ellipse (or in other words its apparent diameter), and P_m is the perimeter of the unconstrained tube. From A_0'', the areas in other states may be obtained by $A' = A_0'' + \Delta A'$, where $\Delta A' = \pi r^2 \Delta h/e$ (Δh being the variation of h). This simple formula does not account for the contribution of the collapsible tube entry zones to variations in air volume. But this contribution is small since the vertical height of these entry zones is less than 4% of e. Moreover, in our experimental range, $h - h' \leqslant 2$ cm and this means that there is very little difference between the pressure inside the collapsible tube and atmospheric pressure. Therefore volume variations related to the compressibility of air are negligible when compared with those related to the capacity of the collapsible tube. The results of these

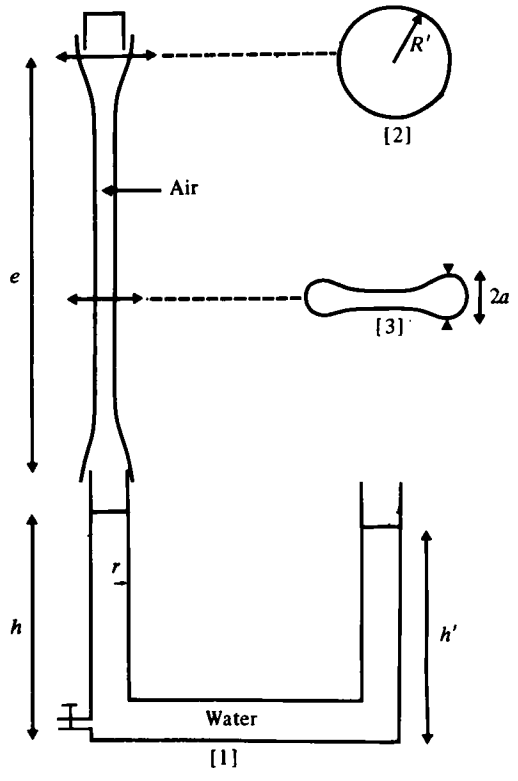

FIGURE 3. Diagram of the experiment making it possible to obtain a relationship between the cross-sectional area of the collapsible tube and its apparent diameter. The results of these measurements are plotted in figure 4.

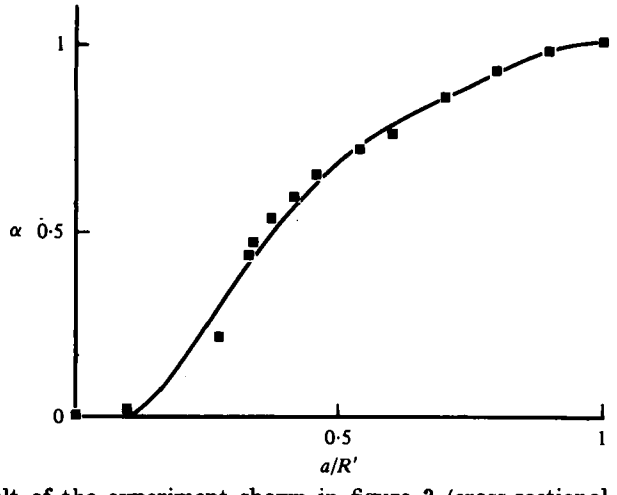

FIGURE 4. Result of the experiment shown in figure 3 (cross-sectional area versus apparent diameter). $\alpha = A'/\pi R'^2$. The two upper points are computed assuming that, at low positive transmural pressure, the horizontal cross-section of the collapsible tube changes from a circular shape (radius R') to a slightly elliptical, unconstrained shape. The two lower points are computed assuming that, at high negative transmural pressures, the collapsible tube is simply opened by two small circular cylinders. The other points are measured ones. The curve is a fifth-degree polynomial fitting the data.

measurements, concerning cross-sectional area versus apparent diameter, are plotted in figure 4.

The changes in slope of the curve area versus apparent diameter correspond to precise events (figure 2): (i) the transition, in cross-section, from elliptical shape to a two-lobed shape; (ii) the onset of line contact between the opposite sides of the tube wall (curve 5 in figure 2).

The relative inaccuracy which resulted from the measurements of the horizontal section areas of the collapsible tube was about 7 %.

3. Theory

3.1. *Fluid motion in the rigid tube, without any flexible tube fastened to its lower end*

The value for the frequency parameter, α, is about 20 in the experimental conditions of the present model. Thus, the velocity profile in the rigid tube can be considered to be approximately blunt.

Conservation of mass in the tank yields

$$A_0 V_0 = (A_1 - A_0) V_1, \tag{1}$$

where A_0 is the area of the horizontal cross-section of the rigid tube, A_1 the area of the horizontal cross-section of the tank, V_0 the fluid cross-section-averaged velocity inside the rigid tube, V_1 the velocity of the free surface of water in the tank (figure 5).

We can also assume that the submersion length, l, of the rigid tube under the water level in the tank is a constant, this level being approximately constant. Indeed, in the hydromechanical model in which $A_0 \ll A_1$ ($A_0 \simeq 10^{-3} A_1$), $\Delta l/l$ is always smaller than 10^{-2}.

It is possible to compute the cross-section-averaged velocity of the fluid column inside the rigid tube during its fall, if the pressure P_c of the fluid within the tank, and the pressure P_0 at the lower end of the rigid tube are known and related. However it is not correct in this case merely to use Bernouilli's equation.

We can, however, notice that (i) at high Reynolds number, due to the boundary-layer separation, there is no curvature of the jet streamlines past the tube; (ii) in a tank where $A_0/A_1 \ll 1$, the average velocity of the fluid is very small compared with the velocity of the jet, and, moreover, the dynamic head of the jet is dissipated in this tank. The inertial effects in the tank are therefore negligible when compared with the hydrostatic effects.

Two assumptions may then be put forward.

(1) The pressure P_0 at the lower end of the rigid tube is approximately equal to the pressure in the tank at the same level:

$$P_0 \simeq P_c(l). \tag{2}$$

(2) The pressure in the tank is simply determined by the hydrostatic effect:

$$P_c(l) = P_{\text{atm}} + \rho g l. \tag{3}$$

Moreover, to obtain an expression for P_0, we used Bernouilli's equation for unsteady flow, and applied it to the fluid motion in the rigid tube. We also took the viscous

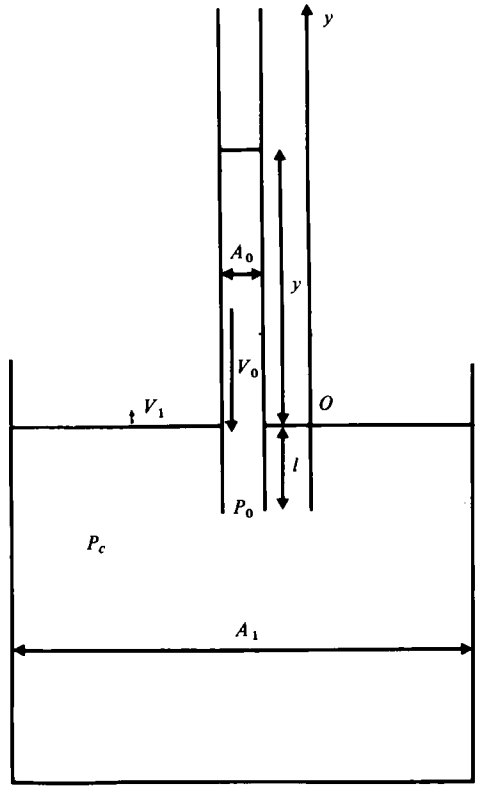

FIGURE 5. Schematic diagram of the tank and the rigid tube.

friction force in the rigid tube to be $f_R = 40\pi\nu\rho V_0(l+y)$. This term is proportional to the cross-section-averaged velocity in the rigid tube and 5 times as great as the one corresponding to the case of a Poiseuille flow profile for the same average velocity. Of course, this last choice is a rough estimate: it should include a proper phase relationship to the velocity. However, at such high Reynolds numbers, the viscous effects cause only a small disturbance, and the expression for f_R is a reasonable approximation.

The expression obtained is

$$P_0 = P_{\text{atm}} + \rho(l+y)\left(g + \frac{dV_0}{dt}\right) + \frac{40\pi\nu\rho}{A_0} V_0(l+y), \tag{4}$$

combining this equation with (2) and (3), we finally obtain

$$\rho(l+y)\frac{dV_0}{dt} + \rho g y + \frac{40\pi\nu\rho}{A_0} V_0(l+y) = 0. \tag{5}$$

This equation, together with $dy/dt = V_0$, was solved by using a fourth-order Runge–Kutta method using dimensionless variables:

$$Y = y/l, \quad Z = V_0/U_0, \quad U_0 = (lg)^{\frac{1}{2}} = l/T, \quad \tau = t/T, \quad T = (l/g)^{\frac{1}{2}}, \quad Re'^{-1} = \frac{40\pi\nu T}{A_0}.$$

The dimensionless initial height of the water in the rigid tube is Y_0/l.

Equation (5) then becomes

$$(1+Y)\frac{dZ}{d\tau}+Y+Re'^{-1}(1+Y)Z=0 \quad \text{with} \quad Z=\frac{dY}{d\tau}. \tag{6}$$

To compute the velocity on the axis of the tube, in an inertia-dominated zone, it is assumed that the same equation can be used, but without any resistive term.

3.2. *Fluid motion in the rigid tube when a collapsible tube is fastened to its lower end*

In this section, we shall try to solve in a simple way the problem of the influence of the short collapsible tube on fluid motion within the rigid tube.

During the acceleration phase, one should consider the flexible tube behaviour as that of a segment of a rigid tube whose radial and longitudinal dimensions are approximately the same as those of this flexible tube when unconstrained. Indeed, the flexible tube is only inflated very slightly even under the highest transmural pressures reached in the present experimental conditions, which are never higher than a few millibars.

During the deceleration phase of the fluid, from the moment when the water level of the rigid tube coincides with that of the tank, the properties of the flexible tube are more difficult to account for, since it is in a collapsing phase.

We nevertheless found that, during this phase, we can physically separate this segment of flexible tube into two zones. The first one is an entry zone, the behaviour of which is strongly determined by being fastened to the lower end of the rigid tube (figure 6*b*).

On the other hand, the second zone is much less constrained and behaves approximately like a collapsible tube uninfluenced by the rigid tube. The difference between the outer and the inner pressure is then expressed by Shapiro's (1977) similitude law:

$$\frac{\Delta P}{\rho U_0^2}=M^{-2}(\alpha_2^{-\frac{3}{2}}-1). \tag{7}$$

where

$$M^{-2}=\frac{K_p}{\rho U_0^2}, \quad \alpha_2=\frac{A_2'}{A_0} \quad \text{and} \quad U_0=(Lg)^{\frac{1}{2}};$$

$K_p=\frac{1}{12}E(h_0/R')^3$ and A_2' is the area of some horizontal cross-section of the second zone of the collapsible tube. In the present case, $M^{-2}\simeq 10^{-2}$. Thus, $\Delta P \ll \rho U_0^2$ for α_2 close to 1. (It should be pointed out that, using the similarity law which is usually valid in a quasi-static case, during the process of fast closure of a collapsible tube, we assume that inertia and viscosity of the wall of the flexible tube are negligible.)

This set of arguments led us to think that the effect of the piece of flexible tube on the motion of the water column in the rigid tube might be represented by an equivalent rigid-tube segment. The length of this equivalent rigid tube is λL, with $\lambda = 1$ during the acceleration phase, and $\lambda \leqslant 1$ during the deceleration phase (figure 6*a*). Although this parameter λ is physically related to the length of the entry zone of the collapsible tube, it must be determined independently, by experimentation. Moreover, the value of the cross-sectional area A_0' of this equivalent rigid tube must also be determined experimentally, though we assume it is close to the unconstrained cross-sectional area of the collapsible tube. We shall now consider the motion of the fluid past the

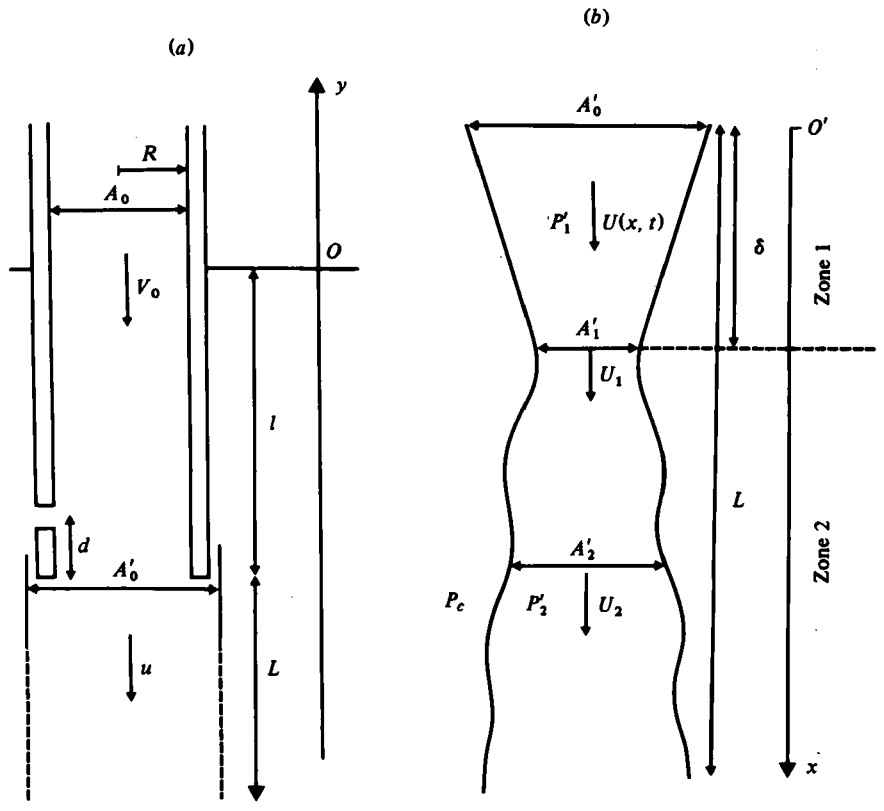

FIGURE 6. (a) Representation of the influence of the collapsible tube upon the upstream flow, by an equivalent rigid tube segment. (b) Diagram of the two zones of the collapsible tube.

sudden enlargement between A_0 and A'_0. Conservation of momentum in the equivalent rigid tube (Batchelor 1967) yields

$$P'_0 = P_0 + \rho\lambda L\left(g + \frac{du}{dt}\right) + \frac{40\pi\nu\rho}{A'_0}u\lambda L + \rho V_0^2\frac{A_0}{A'_0}\left(1 - \frac{A_0}{A'_0}\right), \tag{8}$$

where P'_0 is the pressure at the lower end of the equivalent rigid-tube segment (P_0 is still the pressure at the lower end of the rigid tube) and u is the cross-section averaged velocity of the fluid in the equivalent rigid-tube segment.

Conservation of mass was also taken into account,

$$u = \frac{A_0}{A'_0}V_0, \tag{9}$$

and, if we follow the same reasoning as that leading to equations (2) and (3), we obtain

$$P'_0 = P_{\text{atm}} + \rho(l + \lambda L)g. \tag{10}$$

Combining equations (4), (8), (9) and (10) and using slightly different dimensionless variables (l is replaced by L as the fundamental length) we obtain

$$\left(\frac{l}{L} + Y + \frac{A_0}{A'_0}\lambda\right)\frac{dZ}{d\tau} + Y + \frac{Z}{Re'}\left(\frac{l}{L} + Y + \frac{A_0}{A'_0}\lambda\right) + \gamma Z^2 = 0, \tag{11}$$

in which

$$Z = \frac{V_0}{U_0}, \quad Y = y/L, \quad \gamma = \frac{A_0}{A_0'}\left(1 - \frac{A_0}{A_0'}\right), \quad \tau = t/T,$$

where

$$U_0 = \frac{L}{T} = (gL)^{\frac{1}{2}}, \quad T = (L/g)^{\frac{1}{2}}.$$

This equation was solved like equation (7), using a fourth-order Runge–Kutta method.

The value of λ is 1 during the acceleration phase, so it is initially taken to be 1. When the sign of $dZ/d\tau$ changes, the value of λ is also changed.

Equation (11) is also used, but without any resistive term, to compute the velocity on the axis of the tube.

3.3. *Pressure in the rigid tube*

Using Bernouilli's equation of unsteady flow, we obtain:

$$\frac{P - P_c}{\rho U_c^2} = \left(1 + Y - \frac{d}{l}\right)\left(\frac{dZ}{d\tau} + \frac{Z}{Re'}\right) + Y, \tag{12}$$

where P is the pressure inside the rigid tube at a height d above its lower end and P_c the pressure within the tank at the same level. This equation is obtained assuming that no flexible tube is fastened to the rigid tube. When a flexible tube is fastened to the lower end of the rigid tube, we can derive another equation:

$$\frac{P - P_c}{\rho U_0^2} = \left(\frac{l}{L} + Y - \frac{d}{L}\right)\left(\frac{dZ}{d\tau} + \frac{Z}{Re'}\right) + Y, \tag{13}$$

where Z is the solution of equation (6) in (12), and of (11) in (13).

3.4. *Motion of the collapsible tube*

The geometrical symmetry of the collapsible tube and the mitral valve during the closure process, is predominantly planar. Therefore, in order to describe the closure of the two zones of the flexible tube, we used two-dimensional geometry in the theoretical model. The fluid motion was described by quasi-one-dimensional equations and we also assumed that the vertical height L of the collapsible tube was constant.

The assumption of quasi-one-dimensionality of the fluid motion is valid only if $R'/L \ll 1$. In our experimental case $0{\cdot}1 \leqslant R'/L \leqslant 0{\cdot}2$. These values were chosen because they are small enough to assume quasi-one-dimensionality, while they are not too different from the physiological data. Indeed the ratio of the radial displacement of the anterior mitral leaflet and its longitudinal dimension can be easily determined by taking into account the elliptical shape of the mitral ring: it is about 0·3 (this was estimated using Yacoub's (1976) anatomical data).

(*a*) *First zone of the collapsible tube*

As regards the motion of the first zone of the flexible tube we used a theoretical model derived from that of Van Steenhoven & Van Dongen (1979).

This first zone is assumed to be made of two flat, rigid and inertialess cusps of constant vertical height δ (figure 6*b*).

The continuity equation then yields

$$U(x,t) = \left(-u - \frac{1}{2}\frac{x^2}{\delta}\frac{d\alpha_1}{dt}\right) \Big/ \left(1-(1-\alpha_1)\frac{x}{\delta}\right), \tag{14}$$

where $\alpha_1 = A_1'/A_0'$; A_1' is the cross-sectional area at the lower end of the first zone of the collapsible tube. $U(x,t)$ is the velocity of the fluid within this first zone, at a height x and time t.

It should be noted that $U(0,t) = -u$, because u is the projection of the fluid velocity onto the Oy axis, while $U(0,t)$ is the projection of the same velocity on the $O'x$ axis. These two axes are in opposite directions (see figures 6*a*, *b*). Furthermore, we assumed that, during most of the closure process of the first zone, $(1-\alpha_1) \ll 1$ and $x^2\delta^{-1}d\alpha_1/dt \ll u$. These assumptions are confirmed experimentally and numerically, since the initial value of the function of time α_1 is 1 and its successive derivatives are initially close to 0.

Bernouilli's equation of unsteady flow, applied to the fluid within the first zone, yields

$$P_1'(x,t) = P_0 + \tfrac{1}{2}\rho u^2 - \tfrac{1}{2}\rho U^2(x,t) - \rho\frac{\partial}{\partial t}\int_0^x U(x',t)\,dx' + \rho g x. \tag{15}$$

Let us assume that the interior pressure at the lower end of the first zone is the same as the interior pressure at the upper end of the second zone (i.e. $P_1'(\delta,t) = P_2'(\delta,t)$).

According to equation (7), we know that the difference between the inner and the outer fluid pressures at a height x of the second zone may be written as

$$\frac{\Delta P}{\rho U_0^2} = \frac{P_c(x) - P_2'(x,t)}{\rho U_0^2} = M^{-2}(\alpha_2^{-\frac{3}{2}}(x,t) - 1).$$

Since $\alpha_1(t) = \alpha_2(\delta,t)$ it is also possible to write

$$\frac{P_c(\delta) - P_1'(\delta,t)}{\rho U_0^2} = M^{-2}(\alpha_1^{-\frac{3}{2}}(t) - 1). \tag{16}$$

As has been pointed out, the pressure in the tank at a height x is simply

$$P_c(x) = P_c(\delta) - \rho g(\delta - x). \tag{17}$$

The equilibrium of the moments along one of the rigid cusps which constitute the first zone yields

$$\frac{1}{\delta^2}\int_0^\delta [P_1'(x,t) - P_c(x)]\,x\,dx = 0. \tag{18}$$

From equations (16), (17) and (18) we then obtain

$$\frac{1}{\delta^2}\int_0^\delta [P_1'(x,t) - (P_1'(\delta,t) + \rho U_0^2 M^{-2}(\alpha_1^{-\frac{3}{2}} - 1) - \rho g(\delta - x))]\,x\,dx. \tag{19}$$

The term $P_1'(x,t)$ is calculated from equations (14) and (15) and, making the assumption that terms of order $(1-\alpha_1)^2$ and $[(x^2/u\delta)\,d\alpha_1/dt]^2$ are negligible, we obtain a differential equation, directly written in dimensionless variables,

$$\frac{\epsilon^2}{20}\frac{A_0'}{A_0}\frac{d^2\alpha_1}{d\tau^2} = \frac{\epsilon}{4}Z\frac{d\alpha_1}{d\tau} + (1-\alpha_1)\left[\tfrac{1}{6}Z^2\frac{A_0}{A_0'} - \tfrac{1}{8}\epsilon\frac{dZ}{d\tau}\right] - \frac{\epsilon}{6}\frac{dZ}{d\tau} - \frac{1}{2}\frac{A_0'}{A_0}M^{-2}(\alpha_1^{-\frac{3}{2}} - 1). \tag{20}$$

In the same way, when the terms of order 2, $(1-\alpha_1)^2$ and $[(x^2/u\delta)\,d\alpha_1/dt]^2$, are taken into account and the terms of order 3 are neglected, we come to an equation with a better approximation:

$$\epsilon^2\frac{A_0'}{A_0}\frac{d^2\alpha_1}{d\tau^2}\left[\tfrac{1}{24}(1-\alpha_1)+\tfrac{1}{20}\right]=-\frac{\epsilon}{6}\frac{dZ}{d\tau}+(1-\alpha_1)\left[\frac{Z^2}{6}\frac{A_0}{A_0'}-\tfrac{1}{8}\epsilon\frac{dZ}{d\tau}+\tfrac{1}{2}\epsilon Z\frac{d\alpha_1}{d\tau}\right]$$
$$+\frac{\epsilon}{4}Z\frac{d\alpha_1}{d\tau}+\frac{\epsilon^2}{12}\left(\frac{d\alpha_1}{d\tau}\right)^2\frac{A_0'}{A_0}+(1-\alpha_1)^2\left[\frac{3}{8}\frac{A_0}{A_0'}Z^2-\frac{\epsilon}{10}\frac{dZ}{d\tau}\right]-\frac{1}{2}\frac{A_0'}{A_0}M^{-2}(\alpha_1^{-\frac{3}{2}}-1). \quad (21)$$

Then, from α_1 it is possible to derive the velocity of the fluid at the lower end of the first zone of the collapsible tube:

$$u_1=\frac{1}{\alpha_1}\left[-Z\frac{A_0}{A_0'}-\tfrac{1}{2}\epsilon\frac{d\alpha_1}{d\tau}\right]. \quad (22)$$

In the above equations

$$\alpha_1=\frac{A_1'}{A_0'},\quad \epsilon=\frac{\delta}{L},\quad u_1=\frac{U(\delta,t)}{U_0},\quad Z=\frac{V_0(t)}{U_0}\quad\text{and}\quad \tau=\frac{t}{T}.$$

Equations (20) and (21) were numerically solved (using a fourth-order Runge–Kutta method) taking the origin of time to be the instant which separates the acceleration phase from the deceleration phase of the fluid column within the rigid tube. In equations (20) and (21) $Z(\tau)$ is a known function which is the solution of equation (11). This computation stops when $Z(\tau)=0$, i.e. when $\tau=\tau_2$. The length δ (and thus the parameter ϵ) is determined experimentally, as being the length between the lower end of the rigid tube and the point where the collapsible tube cross-sectional area is minimal.

(*b*) *Second zone of the collapsible tube*

We assume that the second zone is made of two flexible, inertialess, and two-dimensional leaflets. Furthermore we assume that these leaflets are not submitted to any longitudinal stress and that their vertical height, $L-\delta$, is constant.

The quasi-one-dimensional equations of motion can be written, with dimensionless variables, as follows:

$$\frac{\partial u_2}{\partial\tau}+u_2\frac{\partial u_2}{\partial X}=-\frac{\partial p_2}{\partial X}-Re'^{-1}\frac{u_2}{\alpha_2},\quad \frac{\partial\alpha_2}{\partial\tau}+\frac{\partial(\alpha_2u_2)}{\partial X}=0, \quad (23)$$

where

$$u_2=\frac{U_2(x,t)}{U_0},\quad \alpha_2=\frac{A_2'}{A_0'},\quad X=\frac{x}{L},\quad p_2=\frac{P_2'}{\rho U_0^2}.$$

Also $p_c-p_2=M^{-2}(\alpha_2^{-\frac{3}{2}}-1)$. Therefore the first equation (23) becomes

$$\frac{\partial u_2}{\partial\tau}+u_2\frac{\partial u_2}{\partial X}=-\tfrac{3}{2}M^{-2}\alpha_2^{-\frac{1}{2}}\frac{\partial\alpha_2}{\partial X}-Re'^{-1}\frac{u_2}{\alpha_2}. \quad (24)$$

The second equation (23) and equation (24) were simultaneously solved by a finite-difference method. To be more precise the numerical method is based upon an upwind, one-step, explicit, two-time level differencing scheme (Roache 1972).

The initial conditions for the integration of those equations are the following:

$$\alpha_2(X,\tau_1)=1,\quad u_2(X,\tau_1)=-Z(\tau_1)\,A_0/A_0', \quad (25)$$

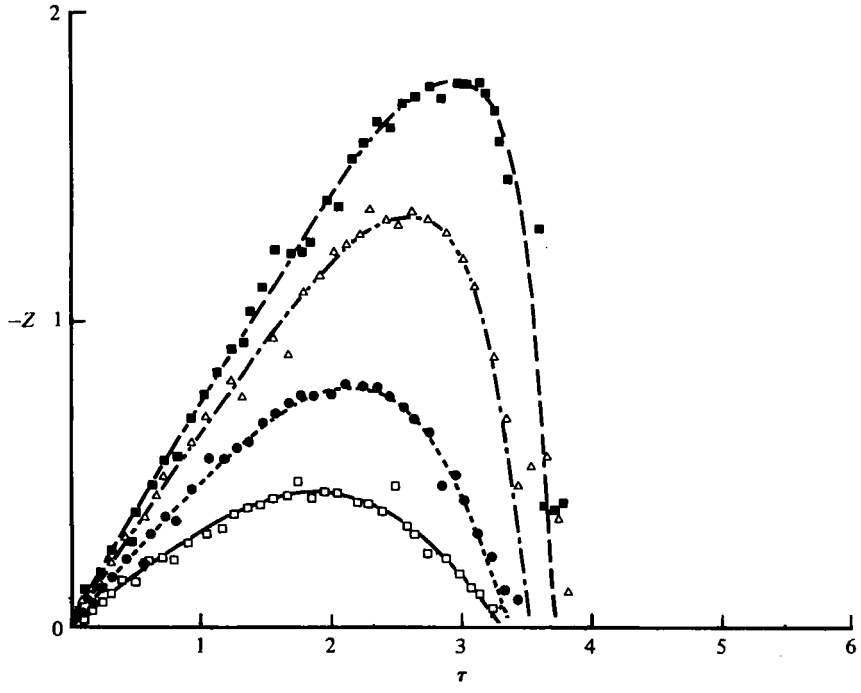

FIGURE 7. Fluid velocity upon the axis of the rigid tube, for several values of Y_0/l. In this case there is not any collapsible tube fastened to its lower end. ——, □, $Y_0/l = 0{\cdot}5$; – – –, ●, $Y_0/l = 1$; — — —, △, $Y_0/l = 2$; — — — —, ■, $Y_0/l = 3$. The curves are computed and the points represent measurements.

where τ_1 is still the instant which separates the acceleration phase from the deceleration phase. Equations (25) indicate that, at the initial instant τ_1, the second zone is uniformly open and that the velocity of the fluid within it is uniform and equal to the entry velocity. The boundary conditions are continuity conditions between the lower end of the first zone and the upper end of the second zone:

$$\alpha_2(\epsilon, \tau) = \alpha_1(\tau), \quad u_2(\epsilon, \tau) = u_1(\tau). \tag{26}$$

4. Results

4.1. *Velocity and pressure within the rigid tube without any flexible tube being fastened to its lower end*

The velocity of the fluid within the rigid tube (on its axis) is theoretically determined and compared with the corresponding experimental data. Figure 7 shows velocity curves as a function of time, for several initial heights of the water level within the rigid tube Y_0. This initial height is expressed by means of a dimensionless number, Y_0/l. The instant $\tau = 0$ coincides experimentally with the opening of the electromagnetic gate.

Figure 8 shows a computed pressure curve and the corresponding measurement data. One can see from this figure that the pressure difference between the fluid within the rigid tube and the fluid within the tank, at a height d above the lower end

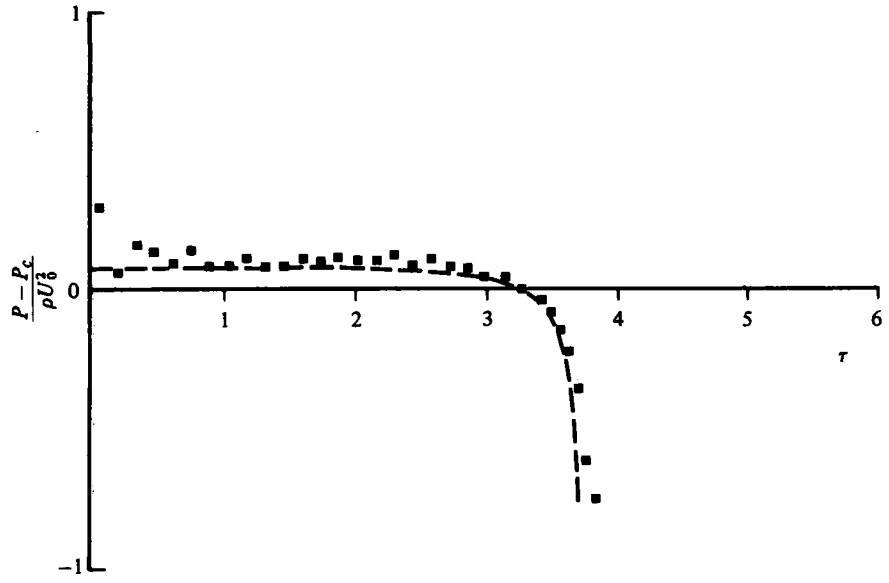

FIGURE 8. Pressure in the rigid tube when there is not a collapsible tube fastened to its lower end. $d/l = 0{\cdot}1$, $Y_0/l = 4$. — — —, computed; ■, measured points.

of the rigid tube, is slightly positive before $\tau = \tau_1$, while it becomes strongly negative from $\tau = \tau_1$ to $\tau = \tau_2$.

The oscillations of the pressure measured when τ is close to 0 are due to the vibrations of the solid support used to hold the hydromechanical model. Apart from this slight problem, there is good agreement between computed and measured data.

4.2. *Velocity and pressure within the rigid tube when a flexible tube is fastened to its lower end*

The shape of the pressure–time curves computed by equation (13) is strongly dependent on the values of λ. So, λ may be experimentally established by comparing these computed curves with the measured points. Figure 9 first shows that the assumption according to which $\lambda = 1$ during the acceleration phase of the fluid is verified by the experimental data when γ is equal to $0{\cdot}2 \pm 0{\cdot}01$, which corresponds to $A_0/A_0' = 0{\cdot}72 \pm 0{\cdot}025$.

During the deceleration phase, some segments of the computed pressure curves are plotted, corresponding to several values of λ. The best fitting between the computed curve and the measured points is obtained when $\lambda = 0{\cdot}6$, in this case where $R'/L = 0{\cdot}1$ and $l/L = 1$. Likewise $\lambda = 0{\cdot}9$ for $l/L = 2$ and $R'/L = 0{\cdot}2$. Therefore, the assumption, according to which the effect of the collapsible tube on the upstream fluid motion can be compared to that of an equivalent rigid tube segment of length λL, becomes experimentally likely.

Figure 10 shows other pressure curves for two values of Y_0. The pressure difference between the fluid within the rigid tube and the fluid within the tank is again measured at a height d above the lower end of the rigid tube. As in the previous case, a collapsible tube is fastened at the end of the rigid tube.

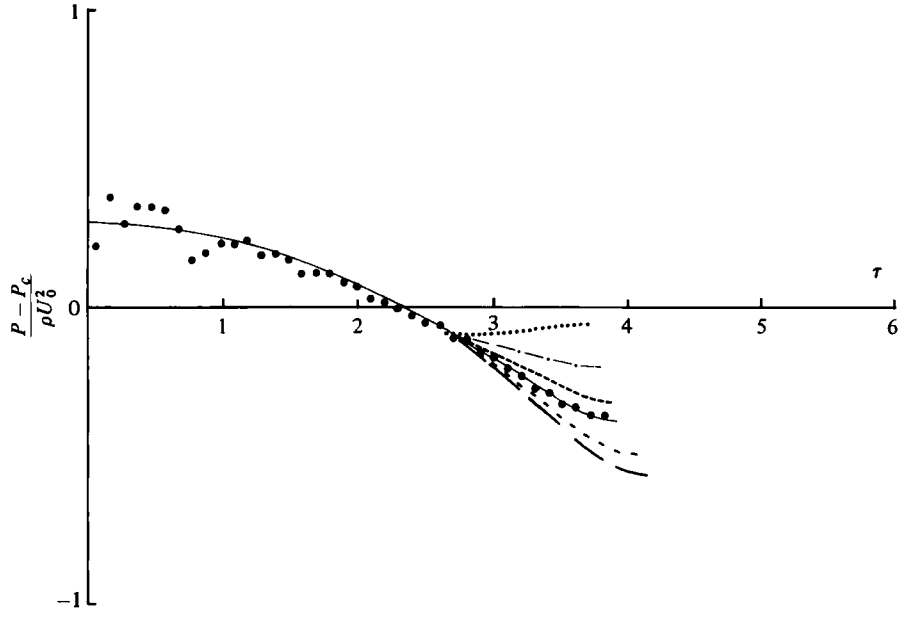

FIGURE 9. Measured points of pressure in the rigid tube, when a collapsible tube is fastened to its lower end. $\gamma = 0{\cdot}21$, $d/L = 0{\cdot}05$, $R'/L = 0{\cdot}1$, $Y_0/L = 1$, $l/L = 1$. The curves were computed from equations (11) and (13), assuming that $\lambda = 1$ during the acceleration phase, and for several values of λ during the deceleration phase: ....., $\lambda = 0$; — — —, $\lambda = 0{\cdot}2$; - - - - - -, $\lambda = 0{\cdot}4$; ——, $\lambda = 0{\cdot}6$; – – –, $\lambda = 0{\cdot}8$; — — —, $\lambda = 1$.

Figure 11 shows several velocity–time curves, for different values of Y_0/L. The velocity is measured on the axis of the rigid tube, when a collapsible tube is fastened at its end. The good agreement between the theoretical curve and the measurements again shows that our assumptions about the effect of the collapsible tube upon the upstream fluid dynamics are a good framework for the interpretation of such phenomena.

4.3. *Collapsible tube opening area*

Figure 12(*a*, *b*) shows the dimensionless area, α_1, of the lower end of the first zone of the collapsible tube as a function of dimensionless time τ, the instant τ_1 here being taken as the origin of time. The computed curves (equation (21)) are compared with the opening-area measurements (i.e. the observed minimum area). It can be seen that the closure of the collapsible tube is delayed in comparison with the onset of fluid deceleration. Otherwise, there is a good agreement between computed and measured data during the first phase of closure, when α_1 remains very close to 1. On the other hand, the computed curves move progressively away from the measured points during the last phase of closure.

The assumptions that $(1-\alpha_1) \ll 1$ and $(x^2/u\delta)\, d\alpha_1/dt \ll 1$ might at least partly explain this progressive divergence. Some other neglected terms, such as longitudinal tension of the tube due to the frictional forces exerted on its wall, may also be of some importance in the late stages of the closure process. The computation was stopped at the instant τ_2 when the fluid velocity within the rigid tube became equal to zero. It was noticed that, experimentally as well as theoretically, closure of the collapsible

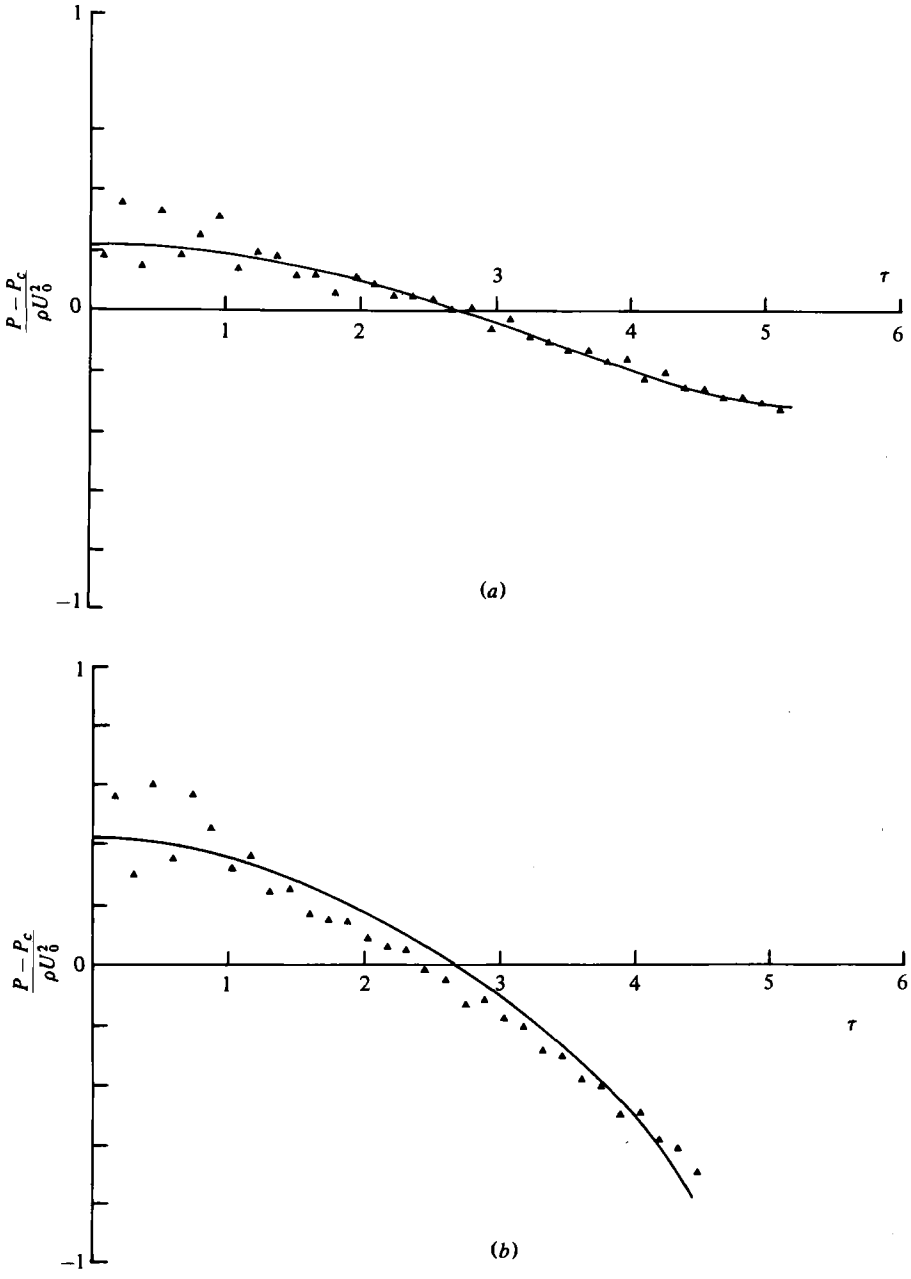

FIGURE 10. Pressure in the rigid tube (when a collapsible tube is fastened to its lower end) for two values of Y_0/L. $R'/L = 0{\cdot}2$, $d/L = 0{\cdot}1$, $\lambda = 0{\cdot}9$, $l/L = 2$. (*a*) $\gamma = 0{\cdot}2$, $Y_0/L = 1$. (*b*) $\gamma = 0{\cdot}21$, $Y_0/L = 3$. ——, computed; ▲, measured.

tube is not completed at this instant. This means that a small amount of regurgitated fluid is necessary to complete the closure, as was already pointed out by Bellhouse (1972) and Lee & Talbot (1979) in their models. Figure 12 also shows polynomials fitting the experimental data, in addition to the theoretical curves. These polynomials allowed us to use, as a boundary condition at the upper end of the second zone of the

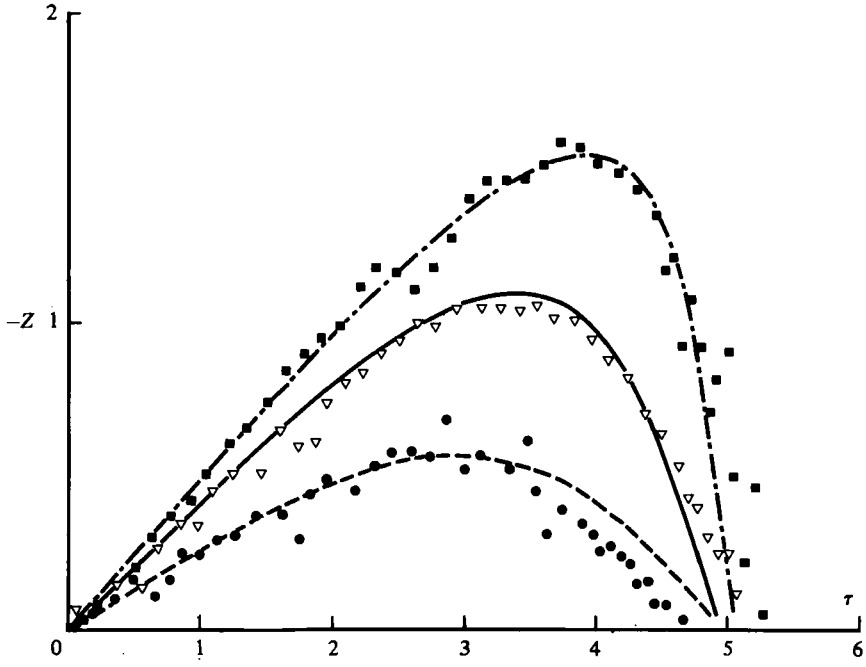

FIGURE 11. Fluid velocity on the axis of the rigid tube for some values of Y_0/L. In this case, a collapsible tube is fastened to its lower end. $\gamma = 0{\cdot}2$, $l/L = 2$, $R'/L = 0{\cdot}2$, $\lambda = 0{\cdot}9$. — — —, ●, $Y_0/L = 1$; ——, ▽, $Y_0/L = 2$; — — —, ■, $Y_0/L = 3$. The curves are computed and the points represent measurements.

collapsible tube ($\alpha_2(\epsilon, \tau) = \alpha_1(\tau)$), a function $\alpha_1(\tau)$, which agrees closely with the measurements. The function $u_1(\tau)$, used as a boundary condition at the upper end of this second zone, is computed by the equation (22), in which $\alpha_1(\tau)$ is the function which agrees with the measurements, and $Z(\tau)$ is the solution of equation (11) until the instant τ_2. For $\tau > \tau_2$, $Z(\tau) = 0$. After closure, the collapsible tube reopens, and this reopening process, which is not studied here, is much slower than the closure process.

4.4. *Collapsible tube profiles*

Figure 13 (*a*, *b*) shows the collapsible tube longitudinal profiles at different times during the closure process. There is good agreement between the experimental data and the computed curves. One can see that the assumption according to which the collapsible tube may be separated into two physical zones seems to be justified experimentally. During the main part of the closure process, the vertical height of the first zone is constant as was assumed previously. However, from figure 13 (*a*) it is clear that at the end of the closure process the vertical height of the entry zone is considerably shortened. This last fact may be related to some features of the phenomena which were neglected in our theoretical description. In particular, we did not take into account the longitudinal tension generated by the viscous friction of the fluid on the wall of the collapsible tube.

The fluid velocity inside the collapsible tube decreases dramatically or is even reversed at the end of the closure process; thus longitudinal tension decreases and

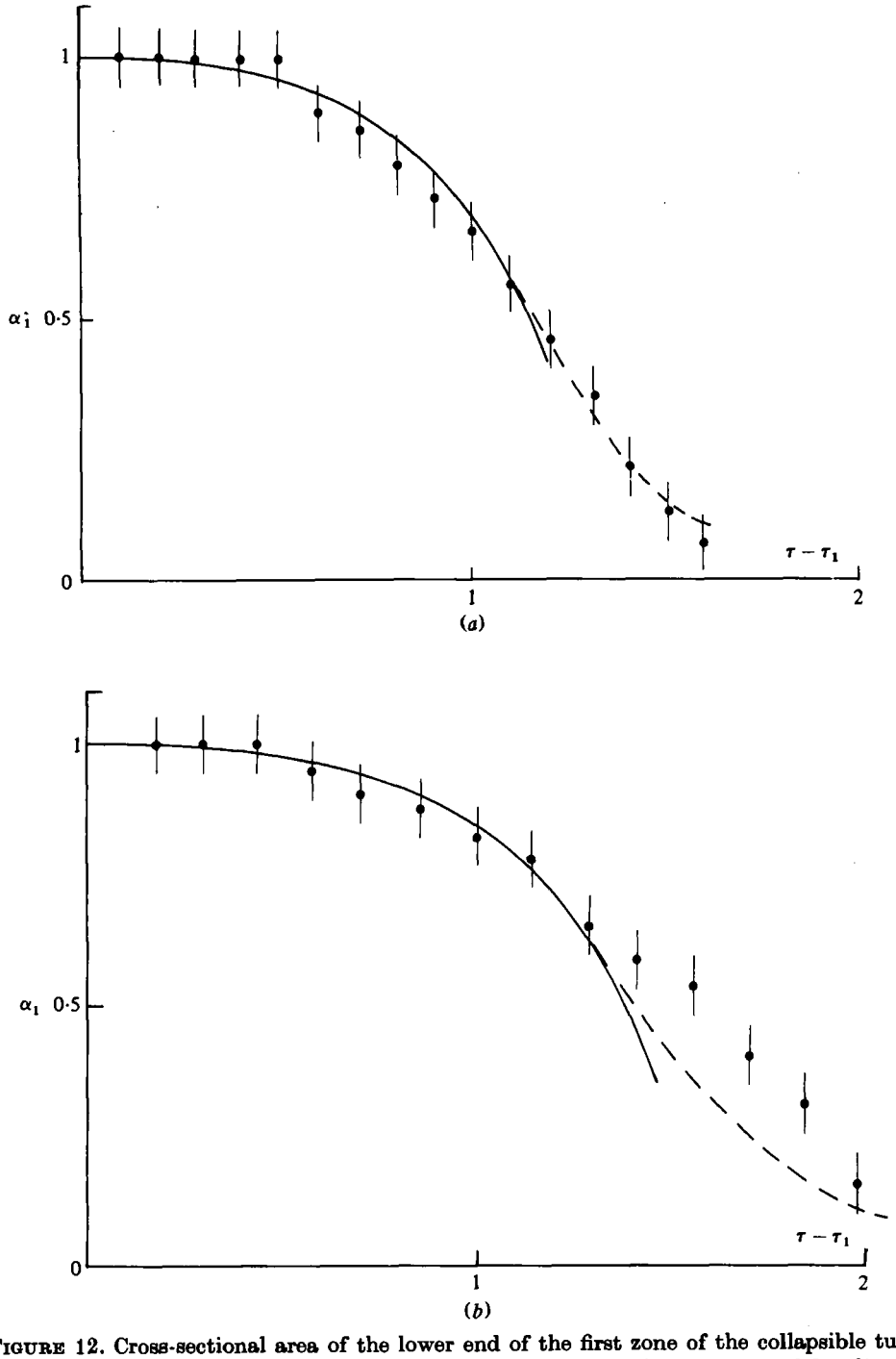

FIGURE 12. Cross-sectional area of the lower end of the first zone of the collapsible tube as a function of time. (*a*) $\gamma = 0{\cdot}2, l/L = 1, R'/L = 0{\cdot}1, \lambda = 0{\cdot}6, Y_0/L = 1{\cdot}5, \epsilon = 0{\cdot}35$. (*b*) $\gamma = 0{\cdot}2, l/L = 2, R'/L = 0{\cdot}2, \lambda = 0{\cdot}9, Y_0/L = 3, \epsilon = 0{\cdot}5$. ●, measured; ——, theoretical; – – –, polynomial.

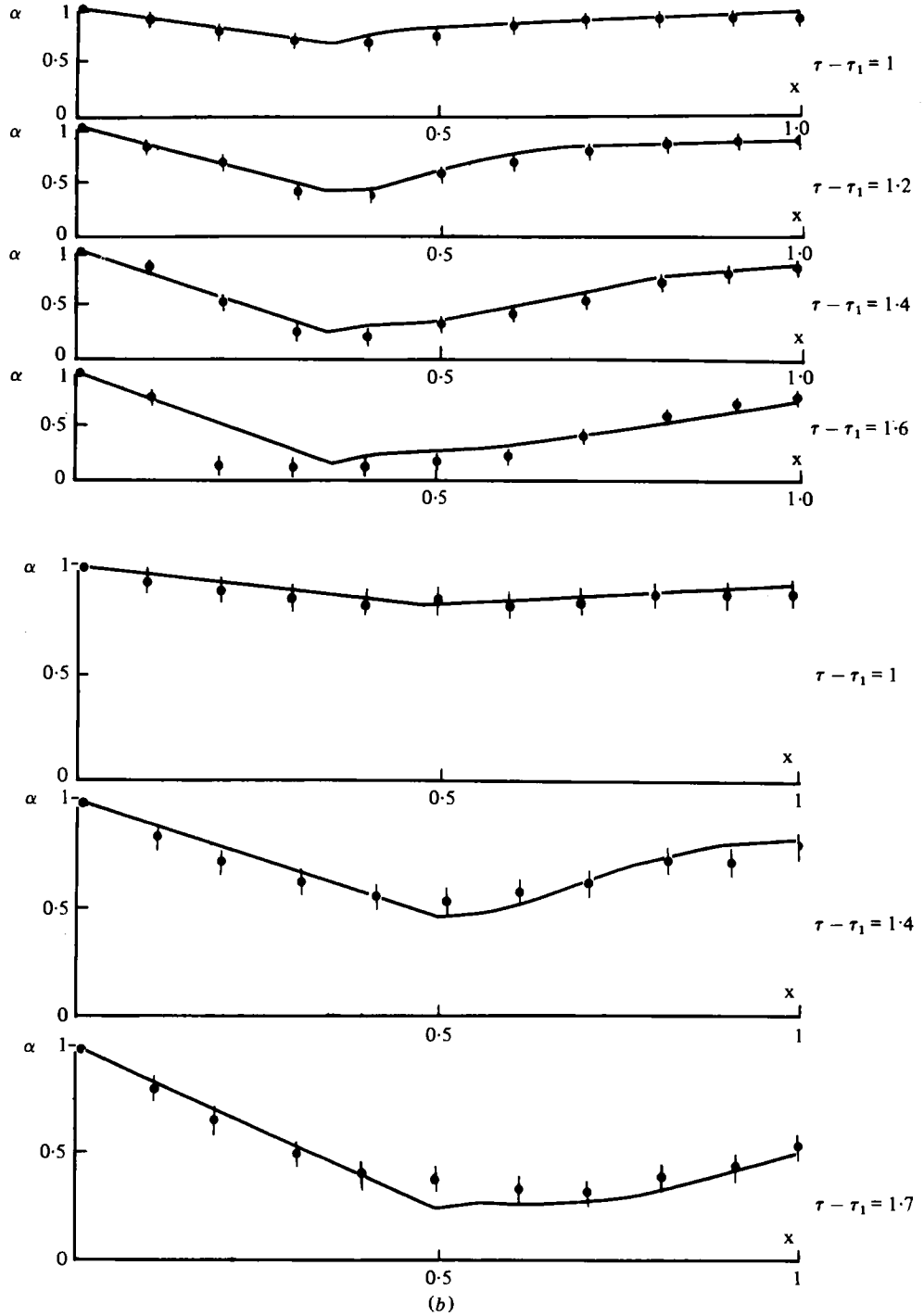

(*b*)

FIGURE 13. Collapsible tube longitudinal profiles at different times. The two zones are plotted. (*a*) $\gamma = 0{\cdot}2$, $l/L = 1$, $R'/L = 0{\cdot}1$, $\lambda = 0{\cdot}6$, $Y_0/L = 1{\cdot}5$, $\epsilon = 0{\cdot}35$. (*b*) $\gamma = 0{\cdot}2$, $l/L = 2$, $R'/L = 0{\cdot}2$, $\lambda = 0{\cdot}9$, $Y_0/L = 3$, $\epsilon = 0{\cdot}5$. The α-scale in (*b*) is doubled with respect to (*a*) in order to show that in this case $R'/L = 0{\cdot}2$, whereas in (*a*) $R'/L = 0{\cdot}1$. ●, measured; ——, computed.

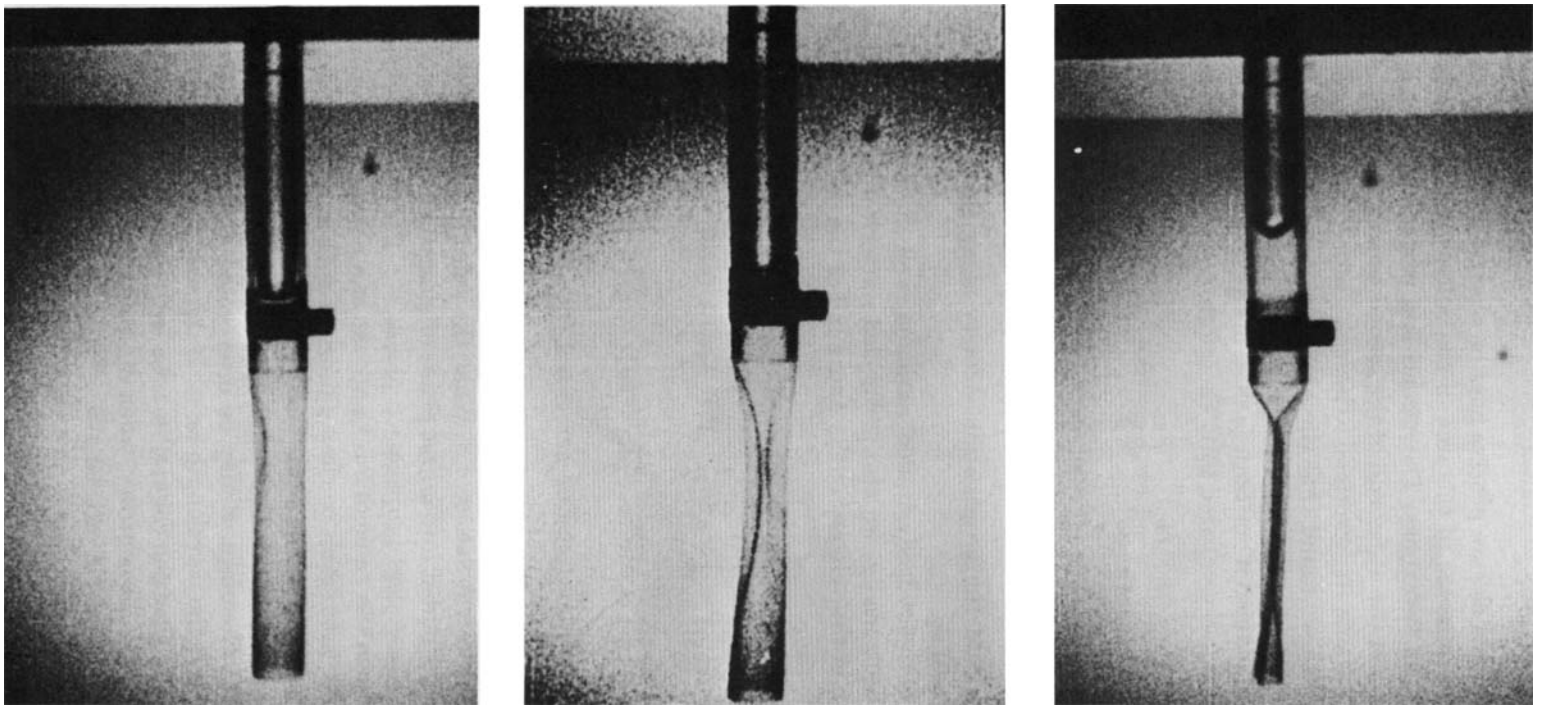

t = 70 ms t = 113 ms t = 196 ms

FIGURE 14. Ciné pictures of the motion of the collapsible tube during the deceleration phase. $t = 0$ is, in this case, the moment when the fluid begins to decelerate. $L = 10$ cm, $l = 10$ cm, $Y_0 = 15$ cm, $S = 1$. The mode of closure is two-lobed and the filming angle is slightly oblique with regard to the collapsing plane (as shown in figure 2).

this might facilitate the process of the entry zone collapse under the effect of transmural pressure.

One should note that the closure process may be separated into two main phases. The first consists of the decrease of the area of the collapsible tube cross-section at the junction between the two zones. The second is a propagation phase, since the closure which originates at the upper end of the second zone of the collapsible tube is propagated along it, towards its lower end. This can also be observed on the photographs of figure 14. We have found that the propagation velocity along the second zone of the collapsible tube is very close to the local velocity of the fluid itself. This last fact can easily be explained if one notices that, in equation (24), the terms of order M^{-2} and Re'^{-1} are very small compared to 1. Therefore, equation (24) may be written approximately as

$$\frac{\partial u_2}{\partial \tau} + u_2 \frac{\partial u_2}{\partial X} = 0.$$

Indeed this type of equation has an analytical solution (Bellman, Cherry & Wing 1958), which is

$$u_2 = f(z) \quad \text{with} \quad z = X - u_2 \tau.$$

It is therefore evident that the propagation velocity along the second zone of the collapsible tube is close to u_2.

To study the effect of the hydrodynamical parameters on the longitudinal shape of the collapsible tube theoretically, we also performed numerical computations using a simple time variation in the velocity at the upper end of the collapsible tube (entry velocity).

Let us assume a flow deceleration model of the following form:

$$Z\left(\frac{t}{T}\right) = \frac{4}{S}\cos 2\pi \frac{t}{T} \quad \text{for} \quad \frac{t}{T} \in [0,\ 0{\cdot}25]$$

$$Z\left(\frac{t}{T}\right) = 0 \quad \text{for} \quad \frac{t}{T} > 0{\cdot}25,$$

where S is the Strouhal deceleration number, $S = L/U_{\max} T_D$, T_D being here equal to $\frac{1}{4}T$; $\tau = t/T$.

Figure 15 shows the theoretical longitudinal shape of the collapsible tube at the same moments, for two different values of S. When the value of S is large enough, the closure process is clearly divided into a first phase of closure motion at the junction of the two zones and a subsequent propagation phase.

On the other hand, when the value of S is small, the two phases merge into a single one. Then the collapsible tube seems to close uniformly with a regular shape.

This may be explained by noticing that, since the wave propagation velocity on the second zone of the collapsible tube is close to the local fluid velocity, $U_{\max} T_D$ is close to the wavelength. Therefore, S may be interpreted as the ratio between the collapsible tube length and the wavelength on it. If the value of S is a small one, the wavelength is much larger than the collapsible tube length and thus the flexible tube seems to close uniformly. On the contrary, when the value of S is close to 1, the wavelength is of order of the collapsible tube length.

Such variations of the Strouhal number for the mitral orifice velocity, are probably often reached in physiological or pathological situations, such as tachycardia, blood flow increase or decrease.

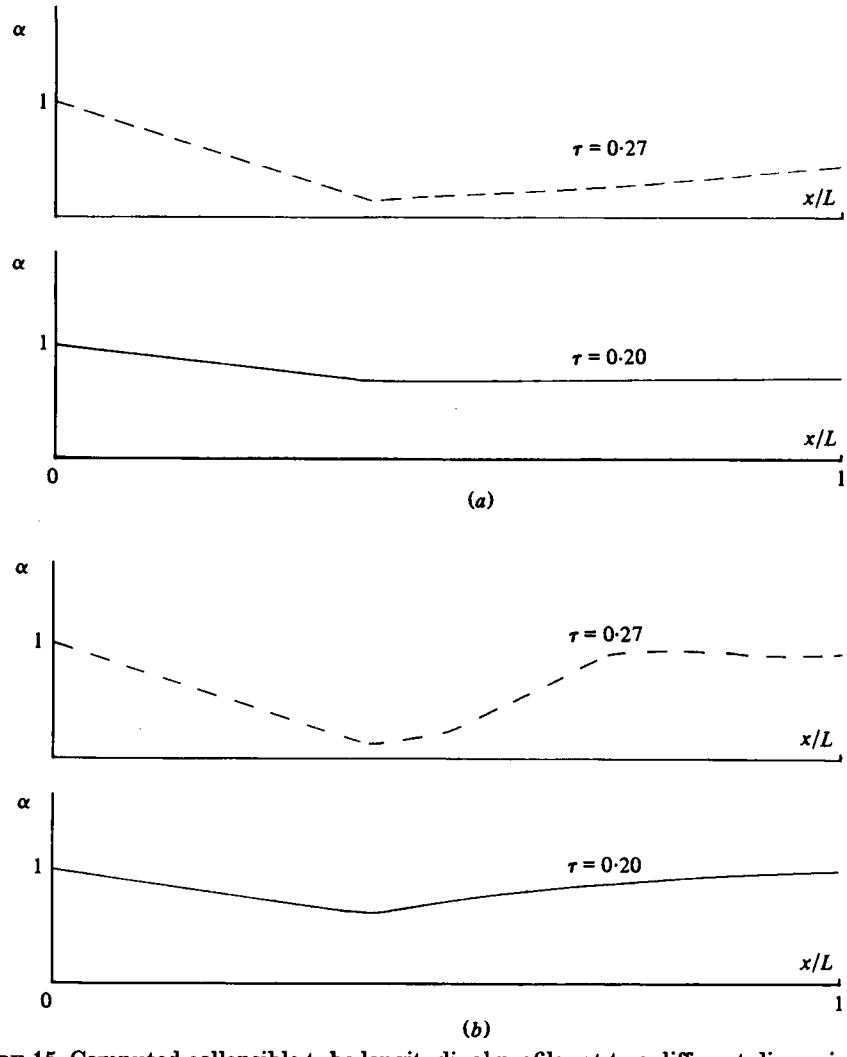

FIGURE 15. Computed collapsible tube longitudinal profiles at two different dimensionless times, for two values of the Strouhal deceleration number. $\epsilon = 0{\cdot}4$, (*a*) $S = 0{\cdot}3$, (*b*) $S = 1{\cdot}2$.

5. Conclusion

During this study, it has been demonstrated that a quasi-one-dimensional model, using very simple assumptions, is an adequate description for the collapsible tube closure process.

It was also possible to conclude that the leading mechanism for the collapsible tube closure is longitudinal flow deceleration. Similar observations were made from the models of Reul & Talukder and Lee & Talbot.

In our case, it is especially important to notice that a complete closure of the flexible tube is achieved in a case where the convective terms in the cavity surrounding the collapsible tube are negligible. As was suggested in the introduction, since in the physiological case $S \geqslant 1$, the convective terms within the cavity surrounding the mitral valve generally have little effect upon its closure motion, though, as has been

demonstrated by Pedley (1980), they may account for the experimental fact that this closure begins before the onset of fluid deceleration (see Laniado & Yellin 1976).

Moreover, the longitudinal shape of the collapsible tube was analysed and it was shown that, after a first phase of closure at the junction between the entry zone and the second zone, a propagation of the perturbed area and fluid velocity takes place in the downstream direction.

The characteristics of this propagation were related to the hydrodynamical parameters of the upstream flow, such as the Strouhal number. It was demonstrated experimentally that the vertical height of the entry zone is approximately constant during the main part of the closure process. Finally, arguments of physical similarity, based upon the estimation of a set of dimensionless numbers, allowed us to establish a close connection in the closure processes between the mitral valve and our Henderson–Johnson-type model.

Therefore, it is possible to extend the main features of the conclusions of the hydromechanical model to mitral-valve motion, especially the most specific aspect of this work: the longitudinal profiles of the collapsible tube. Our knowledge of the relationship between the haemodynamic parameters and the longitudinal profile of a valve leaflet during the closure phase should be very useful in clinical applications, taking into account the recent advances in ultrasound imaging techniques. However, further studies remain to be carried out to specify the effect of pressure and flow fields within the ventricular cavity, as well as that of the longitudinal tension exerted by the chordae, upon mitral valve motion.

The authors acknowledge the helpful suggestions of the referees. This work was supported by the Délégation Générale à la Recherche Scientifique et Technique, contract no. 7872590.

REFERENCES

BATCHELOR, G. K. 1967 *An Introduction to Fluid Dynamics*. Cambridge University Press.

BELLHOUSE, B. J. 1972 The fluid mechanics of heart valves. In *Cardiovascular Fluid Dynamics* (ed. D. H. Bergel), vol. 2, p. 261. Academic.

BELLHOUSE, B. J. & TALBOT, L. 1969 The fluid mechanics of the aortic valve. *J. Fluid Mech.* **35**, 721.

BELLMAN, R., CHERRY, I. & WING, G. M. 1958 A note on the numerical integration of a class of nonlinear hyperbolic equations. *Quart. J. Appl. Math.* **16**, 181.

BITBOL, M. 1980 Modèle hydromécanique de la dynamique de la valve cardiaque. Thèse de 3ème cycle, Université Paris VI.

BITBOL, M., DANTAN, PH., PERROT, P., BRUN, P. & ODDOU, C. 1979 Modèle de l'interaction entre écoulement instationnaire et tuyau collabable court: application à la dynamique de la valve mitrale. Presented at *4ème Congrès de la Société de Biomécanique, Lille.*

BRUN, PH., ODDOU, C., KULAS, A. & LAURENT, F. 1977 Small computer development of echographic information related to left ventricle and mitral valve in diastole. *Computers in cardiology* 1977, p. 267.

BRUN, PH., ODDOU, C., DANTAN, PH., LAPORTE, J. P., LAURENT, F. & PERROT, P. 1980 Blood flow dynamics during the human left ventricular filling phase. In *Cardiac Dynamics* (ed. J. Baan, A. C. Arntzenius & E. L. Yellin), pp. 169–181. The Hague: Martinus Nijhoff.

FLAHERTY, J. E., KELLER, J. B. & RUBINOW, S. I. 1972 Post buckling behaviour of elastic tubes and rings with opposite sides in contact. *SIAM J. Appl. Mech.* **23** (4), 446.

GILLANI, N. V. 1974 Time dependent laminar incompressible flow through a spherical cavity. D.Sc. dissertation, Washington University.

GILLANI, N. V. & SWANSON, W. M. 1976 Time dependent laminar incompressible flow through a spherical cavity. *J. Fluid Mech.* **78**, 99.

HENDERSON, Y. & JOHNSON, F. E. 1912 Two modes of the closure of the heart valves. *Heart* **4**, 69.

LANIADO, S. & YELLIN, E. L. 1976 Simultaneous recording of mitral valve echogram and transmitral flow. In *The Mitral Valve* (ed. D. Kalmanson), pp. 155–162. Edward Arnold.

LEE, C. S. F. & TALBOT, L. 1979 A fluid mechanical study of the closure of heart valves. *J. Fluid Mech.* **91**, 41.

ODDOU, C., DANTAN, P., FLAUD, P. & GEIGER, D. 1979 Aspects of hydrodynamics in cardiovascular research. In *Quantitative Cardiovascular Studies* (ed. N. H. C. Hwang, D. R. Gross & D. J. Patel), pp. 457–492. Baltimore: University Park Press.

PEDLEY, T. J. 1980 *Fluid Mechanics of Large Blood Vessels.* Cambridge University Press.

PESKIN, C. 1977 Numerical analysis of blood flow in the heart. *J. Computer Phys.* **25**, 220.

REUL, H. & TALUKDER, N. 1979 Heart valve mechanics. In *Quantitative Cardiovascular Studies* (ed. N. H. C. Hwang, D. R. Gross & D. J. Patel), pp. 527–564. Baltimore: University Park Press.

RIBREAU, C. & BONIS, M. 1978 Propagation et écoulement dans les tubes collabables. Contribution à l'étude des vaisseaux sanguins. *J. Fr. Biophys. & Med. Nucl.* **3**, 153–158.

ROACHE, P. J. 1972 *Computational Fluid Dynamics*, 2nd edn. Hermosa.

SHAPIRO, A. H. 1977 Steady flow in collapsible tubes. *Trans. A.S.M.E.* K, *J. Biomech. Engng*, **99**, 126–147.

VAN STEENHOVEN, A. A. & VAN DONGEN, M. E. H. 1979 Model studies of the closing behaviour of the aortic valve. *J. Fluid Mech.* **90**, 21.

VOGEL, J. A., ROELANDT, J., BOM, N., ZEELENBERG, C., VERBEEK, P. W. & BAYER, T. 1978 Graphic presentation of two-dimensional cardiac structures in motion. In *Computers in Cardiology*, pp. 381–388. I.E.E.E. Computer Society.

VOGEL, J. A., BASTIAANS, O. L., ROELANDT, J. & HONKOOP, J. 1979 Structure recognition and data extraction in two-dimensional echocardiography. *Echocardiology* (ed. C. T. Lancee), pp. 457–567. The Hague: Martinus Nijhoff.

YACOUB, M. 1976 Anatomy of the mitral valve, chordae and cusps. In *The Mitral Valve* (ed. D. KALMANSON), pp. 15–32. Edward Arnold.

YELLIN, E. L., FRATER, W. M., PESKIN, C. & LANIADO, S. 1976 Left ventricular flow patterns and mitral valve motion: animal studies and computer analysis. *Proc. 4th New England Bioengineering Conf.* (ed. S. Saha), pp. 177–180. Pergamon.